

# Optical properties of $\text{MgH}_2$ measured *in situ* in a novel gas cell for ellipsometry/spectrophotometry

J. Isidorsson,<sup>1,\*</sup> I.A.M.E. Giebels,<sup>1,†</sup> H. Arwin,<sup>2</sup> and R. Griessen<sup>1</sup>

<sup>1</sup>*Faculty of Sciences, Department of Physics and Astronomy, Condensed Matter Physics, Vrije Universiteit, De Boelelaan 1081, 1081 HV Amsterdam, The Netherlands*

<sup>2</sup>*Laboratory of Applied Optics, Department of Physics and Measurement Technology, Linköping University, SE-581 83 Linköping, Sweden*

(Dated: March 13, 2022)

The dielectric properties of  $\alpha\text{-MgH}_2$  are investigated in the photon energy range between 1 and 6.5 eV. For this purpose, a novel sample configuration and experimental setup are developed that allow both optical transmission and ellipsometric measurements of a transparent thin film in equilibrium with hydrogen. We show that  $\alpha\text{-MgH}_2$  is a transparent, colour neutral insulator with a band gap of  $5.6 \pm 0.1$  eV. It has an intrinsic transparency of about 80% over the whole visible spectrum. The dielectric function found in this work confirms very recent band structure calculations using the GW approximation by Alford and Chou.<sup>1</sup> As Pd is used as a cap layer we report also the optical properties of  $\text{PdH}_x$  thin films.

PACS numbers: 77.22.Ch, 77.55.+f, 78.20.Bh, 78.66.Nk

## I. INTRODUCTION

Among metal-hydrides<sup>2</sup> the magnesium hydrogen system has always occupied a special place. Magnesium reacts reversibly with hydrogen to form  $\text{MgH}_2$ . It is thus considered to be one of the most important candidates for the reversible storage of hydrogen<sup>3</sup> due to its lightweight, low cost and high hydrogen storage capacity (7.6 wt.% of hydrogen). In spite of the large number of publications on  $\text{Mg-MgH}_2$  only little is known about the intrinsic physical properties of this system. The scarcity of data for  $\text{MgH}_x$  is mainly due to the experimental difficulties encountered when trying to hydride Mg.<sup>4</sup> Nowadays, a great effort is made to improve the hydrogen ab/desorption kinetics by making nanocrystalline  $\text{Mg}^5$  and/or adding e.g. transition metals<sup>6,7,8</sup> by ball milling.

Recent theoretical calculations<sup>9</sup> reproduce that  $\text{MgH}_2$  undergoes various phase transitions<sup>10,11</sup> as a function of pressure. All theoretical calculations published so far<sup>9,12,13,14</sup> (using either the local density approximation (LDA) or the generalized gradient approximation (GGA)) predict band gaps between 3.1 and 4.2 eV for  $\alpha\text{-MgH}_2$ . This is smaller than the few sporadic experimental values reported until now. Krasko<sup>15</sup> mentions a value of 5.16 eV for the band gap from unpublished work by Genossar. He and Pong<sup>16</sup> determined in an indirect way using Penn's formula<sup>17</sup> an average band gap of 5.8 eV. Yamamoto *et al.*<sup>18</sup> report an optical transmission spectrum for a thin film in which the transmission vanishes at 6.05 eV (205 nm). Apart from that Ellinger *et al.*<sup>19</sup> found an index of refraction of 1.95 and 1.96 for the ordinary and extraordinary rays at 589.3 nm. The dielectric properties have not been studied at all. This triggered our interest to study the optical properties of  $\text{MgH}_2$  in detail.

Another strong reason for our interest in  $\text{MgH}_2$  stems from metal-hydride switchable mirrors. In 1996 Hui-

berts *et al.*<sup>20</sup> discovered that Y and La thin films change reversibly from shiny, metallic films to transparent, insulating films upon hydrogenation either by changing the surrounding hydrogen gas pressure or the electrolytic cell potential.<sup>21,22</sup> In 1997 Van der Sluis *et al.*<sup>23</sup> discovered that all rare-earth (RE) metals exhibit such a switchable behaviour. However, all these materials have a characteristic colour in the fully hydrogenated state because their band gap is in the visible ( $E_g < 3$  eV). They showed that alloying with Mg results in colour neutral switchable mirrors. This is very important for applications in e.g. 'smart' windows. In 2001 Richardson *et al.*<sup>24</sup> reported that  $\text{Mg}_z\text{Ni}$  ( $z > 2$ ) also features reversible switching behaviour upon hydrogenation. In all these cases (RE-Mg and  $\text{Mg}_z\text{Ni}$ ), the band gap is shifted to higher energies with increasing magnesium concentration.<sup>23,24,25,26,27</sup> All these alloys disproportionate upon hydrogenation.<sup>25,28,29,30</sup> This disproportionation is also known for bulk RE-Mg.<sup>31,32</sup> The available data suggest that the shift of the band gap to higher energies is due to the formation of  $\text{MgH}_2$  which is expected to have a large band gap. At the same time the reflectance in the low hydrogen phase (when the sample is unloaded) increases due to Mg which has a high reflection.<sup>23,33</sup> At intermediate concentrations the coexistence of Mg and  $\text{MgH}_2$  seems to play an important role in the realization of a highly absorbing, black state that is observed during loading and unloading of RE-Mg alloys.<sup>34,35</sup> It may also play a role in the black state observed in  $\text{Mg}_z\text{NiH}_x$ .<sup>36</sup> Thus, to understand the role of  $\text{MgH}_2$  in Mg-containing switchable mirrors it is essential to determine the optical properties of  $\text{MgH}_2$  thin films.

In this paper we study thin films of magnesium hydride with spectrophotometry and ellipsometry and determine the dielectric function and the optical band gap. For this purpose we use a special substrate geometry and a novel type of optical gas loading cell.

## II. EXPERIMENTAL

MgH<sub>2</sub> thin films are made in two steps. First Pd capped metallic Mg films are deposited under UHV conditions on an appropriate substrate. The Pd cap layer is necessary to protect Mg against oxidation and to promote hydrogen dissociation and absorption. The films are subsequently loaded with hydrogen under high pressure up to the composition MgH<sub>2</sub>.

The hydrogenation of Mg to MgH<sub>2</sub> is, however, not straightforward as was shown by Krozer, Kasemo and others.<sup>37,38,39,40,41</sup> Palladium capped Mg films exhibit unusual kinetics due to the formation of a blocking MgH<sub>2</sub> layer at the interface between Pd and Mg. The MgH<sub>2</sub> layer prevents H to diffuse<sup>42</sup> to the metallic Mg that is still present underneath. The formation of this blocking layer can be circumvented by starting hydrogenation at relatively low (1 mbar) H<sub>2</sub> pressure at a temperature of 100°C. Magnesium films with thicknesses up to 150 nm can be fully transformed to MgH<sub>2</sub> in this way.<sup>39,43</sup>

### A. Film deposition

Thin, polycrystalline films of Mg and Pd are deposited at room temperature in an UHV MBE system with a background pressure of 10<sup>-9</sup> mbar, using material of typically 99.9 % purity. The magnesium films are evaporated from a Knudsen cell and covered with a 10 nm thick Pd cap layer. These palladium films are deposited from an e-beam evaporation unit. Typically, we deposit films simultaneously on a 10x10 mm<sup>2</sup> glassy carbon substrate for Rutherford backscattering spectrometry (RBS), 10x10 mm<sup>2</sup> quartz substrates for X-ray diffraction (XRD), resistivity and/or AFM measurements, and on a quartz substrate (Ø 42 mm, Heraeus Suprasil 1) for optical measurements.

### B. Film characterization

RBS is used to determine eventual contamination of the films. For this glassy carbon substrates are used in order to separate the Mg signal from the background signal of the substrate. An oxygen contamination between  $0.03 \leq [\text{O}]/[\text{Mg}] \leq 0.085$  has been found.

The thickness of the film is measured with a DekTac<sup>3</sup> or a Tencor Alpha step 200 mechanical stylus profilometer. The surface structure, both before and after hydrogen loading, is investigated with a NanoScope III atomic force microscope (AFM), operating in tapping mode using silicon cantilevers. The scanned areas are typically 1x1 and 5x5  $\mu\text{m}^2$  from which the root-mean-square (RMS) roughness is determined. The thickness and roughness values from these techniques are used as input parameters in the modeling of the transmission, reflection and ellipsometric data (see Sec. III).

Some samples are contacted ultrasonically with four 30  $\mu\text{m}$  aluminium wires to monitor the resistivity with the Van der Pauw method<sup>44</sup> during loading with hydrogen.

X-ray experiments are carried out with Cu K $\alpha$  radiation in a Rigaku ‘Rotaflex’ RU 200 or Bruker D8 Discover X-ray diffractometer to monitor the transformation of hcp Mg to rutile MgH<sub>2</sub> in a  $\theta$ -2 $\theta$  mode.

### C. Optical techniques

Optical reflection and transmission measurements at room temperature (RT) are carried out in a Perkin Elmer Lambda 900 spectrophotometer in the range  $0.5 < \hbar\omega < 6.7$  eV ( $2500 > \lambda > 185$  nm). The specular and total transmission is recorded while the spectrophotometer is purged with argon or nitrogen in order to reduce absorption by O<sub>2</sub> in the ultraviolet (UV), and H<sub>2</sub>O in the infrared (IR). The quartz substrates (without film) and Pd samples are measured in reflection geometry from the top side (i.e. the metallic side) at near normal incidence (8°) in an absolute reflection unit (using a so-called VN geometry).

Ellipsometry measurements (at RT) in the energy range 1.0 to 6.5 eV ( $1240 > \lambda > 190$  nm) are carried out in a rotating analyzer variable-angle spectroscopic ellipsometer (VASE, J.A. Woollam Co. Inc.), using the WVASE32 software program for data acquisition and analysis. This instrument measures the ratio of the complex Fresnel reflection coefficients  $R$  of parallel ( $p$ ) and perpendicular ( $s$ ) polarized light.<sup>45</sup> This ratio defines the ellipsometric angles  $\Psi(\omega)$  and  $\Delta(\omega)$  according to

$$\frac{R_p}{R_s} = \tan(\Psi(\omega)) \exp(i\Delta(\omega)) \quad (1)$$

Three angles of incidence (60, 65 and 70°) are used to obtain adequate sensitivity over the whole spectral range. Standard deviation and ellipsometric data ( $\Psi, \Delta$ ) are recorded at each data point as an average of at least 100 revolutions, and up to 4000 revolutions of the analyzer for the most critical data.

### D. Semi-cylindrical substrate

As the Pd cap layer on top of the very transparent MgH<sub>2</sub> layer is strongly absorbing, ellipsometry cannot be carried out from the Pd-side. Thus, ellipsometry measurements need to be performed from the ‘backside’, through the substrate. Flat substrates would need to be so thick that reflections from the front and backside of the substrate can be well separated. With a 2 mm diameter of the light beam the substrate must be thicker than 3 mm. However, at large angles of incidence the intensity loss in the light beam is substantial due to reflections at the air/substrate interface. Furthermore, at energies close to the limit of the ellipsometer (6-6.5 eV),

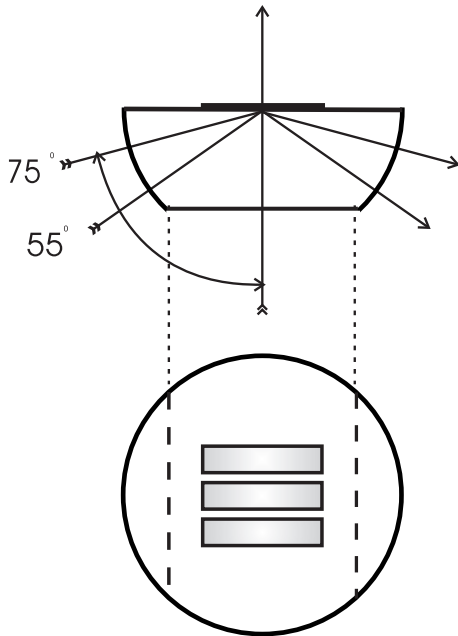


FIG. 1: Semi-cylindrical quartz glass substrate for ellipsometry and transmission measurements. The upper figure is a side view of the substrate, the one on the bottom a top view. A perspective view is given in Fig. 2. The angle of incidence of light can be varied between  $55^\circ$  and  $75^\circ$ . On the flat part of the substrate three samples with different Mg thicknesses are deposited. They are all covered with a 12 nm thick Pd cap layer.

the intensity of the light beam is diminishing quickly. These limitations can be avoided with a semi-cylindrical substrate.

This substrate is designed for normal incidence of light at the ambient/substrate interface and oblique incidence at the internal substrate/MgH<sub>2</sub> interface (see Fig. 1). For the normal incident approximation to be valid, the diameter of the semi-cylindrical substrate must be large compared to the size of the light beam (2 mm). For practical reasons we choose a semi-cylindrical substrate with a diameter of 42 mm. The top part of the semi-cylindrical substrate is cut away parallel to the base surface to enable transmission measurements. This design allows the angle of the incident light onto the sample to vary between  $55^\circ$  and  $75^\circ$  from the normal. Both the flat and the semi-cylindrical substrates are made of quartz glass (Heraeus Suprasil 1). This material is transparent deep into the UV beyond the limit of our ellipsometer and spectrophotometer.

On the top of the large flat face we deposit, under exactly the same condition, three films with different Mg thicknesses (see Fig. 1). This allows us to analyze compositionally identical films. This method makes the determination of the dielectric function from ellipsometric data more reliable.<sup>46,47</sup>

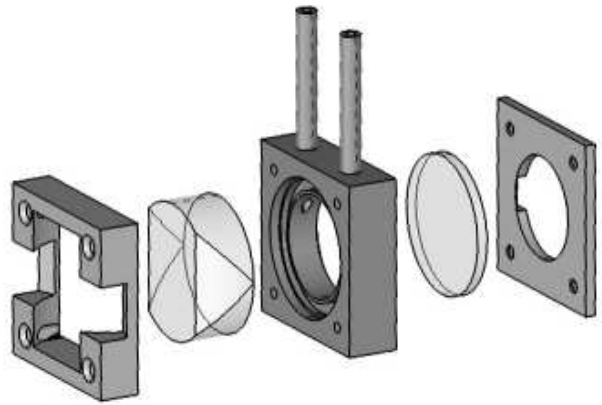


FIG. 2: Exploded view of the optical gas loading cell for *in situ* ellipsometry and transmission measurements in a hydrogen environment. In this sketch the cell is shown with the semi-cylindrical substrate (see Fig. 1) as sample window at the front side. Alternatively, a flat window such as the one at the backside of the cell, can be used as sample substrate.

#### E. Optical gas loading cell and high pressure loading chamber

In order to measure the optical properties of MgH<sub>2</sub> and PdH<sub>x</sub> *in situ* in equilibrium with hydrogen at various pressures, we designed an experimental setup consisting of three parts: i) a substrate/window (see Fig. 1), ii) an optical gas loading cell, and iii) a high pressure loading chamber. Components ii) and iii) are described below in more detail. The setup also includes a special substrate holder with a sliding mask for the deposition of the films, and a holder to attach the optical gas loading cell to the ellipsometer.

A semi-cylindrical or a flat substrate with the Pd-capped MgH<sub>2</sub> films deposited on top functions as window in the optical gas loading cell (see Fig. 2). For ellipsometry the sample/window is illuminated through the substrate to measure the ‘backside’ of the film. For *in situ* transmission measurements a window is mounted on the opposite side of the cell as well. The sample can be exposed to a controlled hydrogen gas atmosphere during the measurements via two tubes connected to a vacuum pump and hydrogen gas cylinder. The cell is designed for vacuum, but works also reliably up to a few bar hydrogen pressure.

As already mentioned in the introduction of Sec. II, hydrogenation of Mg to MgH<sub>2</sub> can be successfully achieved at moderate temperatures (100°C) by starting at low hydrogen pressure.<sup>39,43</sup> Therefore, to be sure that our thin films of Mg are completely transformed to MgH<sub>2</sub> we start loading with a H<sub>2</sub> pressure of 1 mbar and increase it in steps (within a few hours) up to 100 bar H<sub>2</sub>. To do this the optical gas loading cell is mounted inside a high pressure loading chamber (see Fig. 3). This chamber is

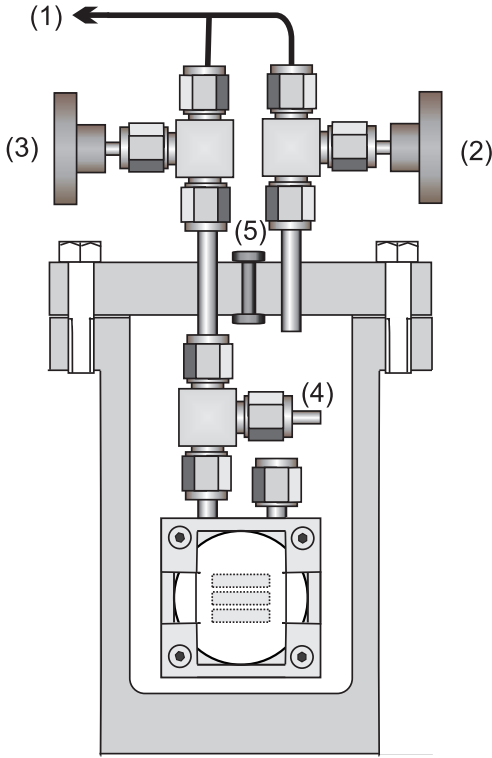


FIG. 3: High pressure chamber to load the Mg samples to  $\text{MgH}_2$  at a pressure of 100 bar  $\text{H}_2$ . The optical gas loading cell shown in Fig. 2 is mounted inside the chamber. The various parts are: (1) connection to the vacuum and gas handling system, (2) a valve to open and close the high pressure chamber, (3) and (4) valves to open and close the optical gas cell, (5) is the electrical feed-through to enable *in situ* measurements of the resistivity and temperature.

made of stainless steel and proof-pressurized to 200 bar. The design is such that the pressure in the high pressure chamber is everywhere the same, and it is not necessary to expose the sample to the ambient after loading at 100 bar  $\text{H}_2$ . It is possible to release hydrogen and close the optical gas loading cell with valve (3) when a pressure of 1 bar hydrogen or less is reached. With valve (2) closed as well, the system is disconnected from the gas tubes (1) (while still filled with  $\text{H}_2$ ). Afterwards, valve (2) is opened to equalize the pressure outside and inside the high pressure chamber. Then, the chamber is opened, and the valve on top of the optical gas cell (number 4) is closed. The cell can then be disconnected from the lid of the high pressure loading chamber while still filled with hydrogen. The high pressure loading chamber is also equipped with an electrical feed-through (5) with several wires to permit measurements of the resistivity of a sample during hydrogenation and of the temperature inside the chamber with a RhFe100 sensor. During hydrogen loading of a Mg film the total chamber can be resistively heated up to 100°C.

### III. RESULTS

#### A. Sample characterization

Since Mg is a metal and  $\text{MgH}_2$  an insulator, the time evolution of hydrogenation can be followed *in situ* in real time by monitoring the change of the resistivity.<sup>48</sup> This allows us to optimize the hydrogen pressure (starting at low pressures and increasing it stepwise to 100 bar  $\text{H}_2$ ) in such a way that no impenetrable  $\text{MgH}_2$  layer is formed at the interface between Pd and Mg. For practical reasons we have mounted an extra sample in the high pressure loading chamber for resistivity measurements.

The resistivity of this as-deposited 150 nm Mg film covered with 15 nm of Pd at RT is  $6.5 \mu\Omega\text{cm}$  (the literature value for bulk Mg at 20°C is  $4.4 \mu\Omega\text{cm}$ <sup>49</sup>). The reflection of this as-deposited film is high in the visible and near-infrared regions ( $\sim 80\%$ ). Both the low resistivity and the high reflection indicate the good quality of the film. After loading the resistivity reaches  $680 \mu\Omega\text{cm}$  under 100 bar  $\text{H}_2$  at 100°C. Since  $\text{MgH}_2$  is an insulator one would at first sight expect a much higher value. The moderate resistivity found experimentally is, however, due to the metallic Pd cap layer that shortcuts the  $\text{MgH}_2$  layer. Moreover, at a temperature of 100°C Mg and Pd may interdiffuse to form a Mg-Pd alloy.<sup>40,50</sup> This intermixing has been suggested for Pd capped Y as well,<sup>51</sup> and was conclusively shown with photoelectron spectroscopy recently.<sup>52</sup> RBS showed an intermixing of Mg and Pd in our films as well. This can be due to either alloying, interface roughening or both. The net result is that a relatively Pd-rich Pd-Mg alloy is formed on top of  $\text{MgH}_2$  that absorbs some hydrogen but does not become insulating and this causes the shortcut.

In the as-deposited metallic state, hcp Mg has a preferential growth direction, and only the (002) reflection is present in the X-ray diffractogram (see Fig. 4(a)). Loading a thin Mg film in 1 bar  $\text{H}_2$  at 100°C does not transform Mg completely to  $\text{MgH}_2$  (see Fig. 4(b)). Loading at 100 bar and 100°C, on the other hand, left no traces of metallic Mg. Only the peaks corresponding to the tetragonal structure of the rutile type<sup>19</sup> of  $\alpha\text{-MgH}_2$  are observed (see Fig. 4(c)). Such a preferred growth direction is not observed for  $\text{MgH}_2$  where weak signals from the (110), (101) and (200) peaks can be seen. Rocking curves around the (002) Mg peak and the (110)  $\text{MgH}_2$  peaks show that our samples are polycrystalline.

AFM measurements revealed a significant difference between the as-deposited Pd covered Mg film and the fully hydrogenated films (see Fig. 5). Mg expands by 32% in volume when transforming from hcp Mg to rutile  $\text{MgH}_2$ .<sup>53</sup> Since the film is clamped by the substrate it cannot expand laterally and all the expansion must take place out-of-plane. With AFM we indeed noted an increase in the RMS roughness from 5 nm to 14 nm. It can be seen as well that our top layer of Pd is cracked. With a mechanical stylus profilometer we found a corresponding increase of the thickness of the film from 113 to

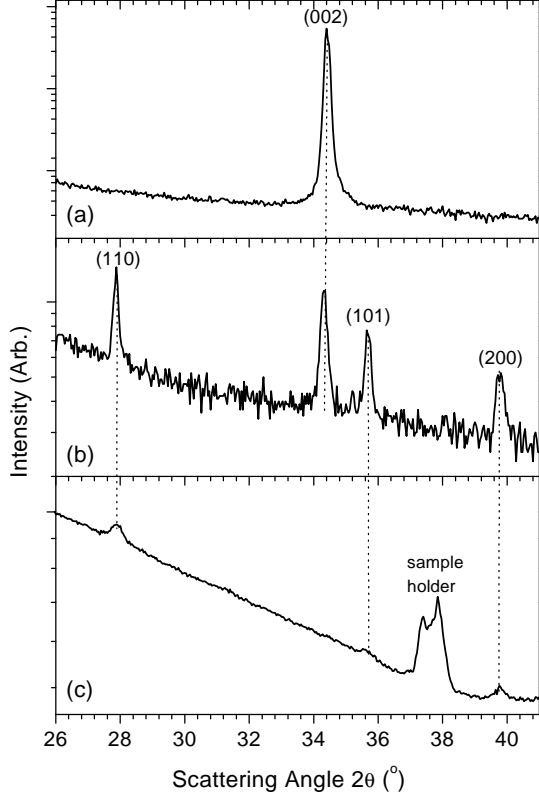


FIG. 4: X-ray diffraction spectra of a 188 nm Mg/10 nm Pd film (a) as-deposited, (b) loaded up to 1 bar  $H_2$  and (c) of a 150 nm Mg/15 nm Pd film loaded up to 100 bar  $H_2$ . The large background is due to the quartz substrate.

162 nm. This 43% increase is larger than the expected 32% volume expansion because the mechanical stylus has a tip radius of  $12.5 \mu\text{m}$ , and hence cannot probe the deep valleys seen on the AFM image. During ellipsometry we look through the substrate at the backside of our films and not from the top side as with AFM. Nevertheless, we found that surface roughening of our Pd top layer needed to be taken into account when modeling the ellipsometric data.

### B. Transmission and band gap of $\text{MgH}_2$

The optical transmission of Pd capped  $\text{MgH}_2$  films is measured *in situ* in 1 bar  $H_2$  using the gas loading cell (see Fig. 2). Figure 6 shows the total, specular and diffuse transmission of a 150 nm thick  $\text{MgH}_2$  film capped with 12 nm Pd, loaded at 100 bar  $H_2$  and  $100^\circ\text{C}$ . The total transmission is measured with the optical gas loading cell placed at the entrance port of the integrating sphere in the spectrophotometer. In this experiment a flat 3 mm thick quartz glass substrate is used. Since we look at our film from the substrate side, the  $\text{MgH}_2$  layer is situ-

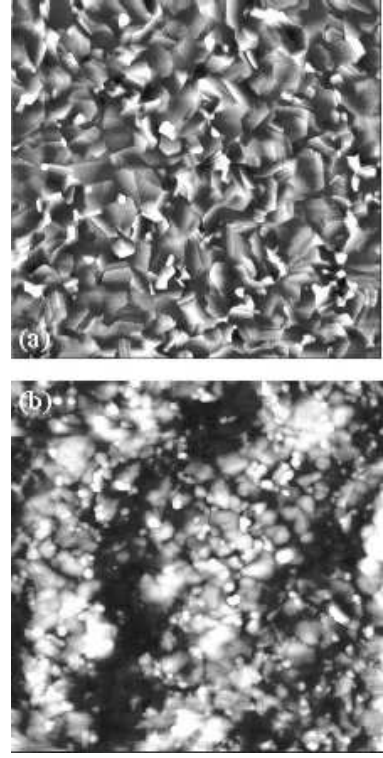


FIG. 5: AFM images of the surface ( $5 \times 5 \mu\text{m}^2$ ) of a 101 nm Mg/12 nm Pd (a) as-deposited (b) after loading with hydrogen at 100 bar. The root mean square roughness increases from 5 to 14 nm due to the 32% volume expansion accompanied by the transition from hcp Mg to rutile  $\text{MgH}_2$ .

ated 3 mm away from the port of the integrating sphere. The specular transmission is measured with the sample in the sample compartment, using the direct detector to monitor the signal. The difference between these two signals is the diffuse (scattered) transmission. It is probably due to the rough surface (see Sec. III A and Fig. 5(b)) of our loaded samples. This diffuse transmission,  $T_d$ , has a strong wavelength dependence and is proportional to

$$T_d \propto \frac{1}{\lambda^4} \propto (\hbar\omega)^4, \quad (2)$$

where  $\lambda$  is the wavelength of light.<sup>54</sup> It is clear from Fig. 6(b) that the diffuse transmission decreases strongly above the band gap as the film starts to absorb light. The optical band gap  $E_g$ , can be estimated from the intersection of a fitted  $(\hbar\omega)^4$  curve to the data and an extrapolation of the flank of the absorption edge. Using this so called ‘Rayleigh method’ we find  $E_g = 5.61 \text{ eV}$  for this sample and  $E_g = 5.67 \text{ eV}$  for a second sample.

Another estimate for  $E_g$  can be obtained from the absorption edge of the transmission spectra using the Lambert-Beer law,  $T(\omega) = T_0 \exp[-\alpha(\omega)d]$ , where  $\alpha$  is the absorption coefficient,  $d$  the film thickness and  $T_0$  contains the transmission of the Pd cap layer and the quartz substrate. In the region of the absorption edge  $T_0$  can be considered as constant in our films (see Figs. 7

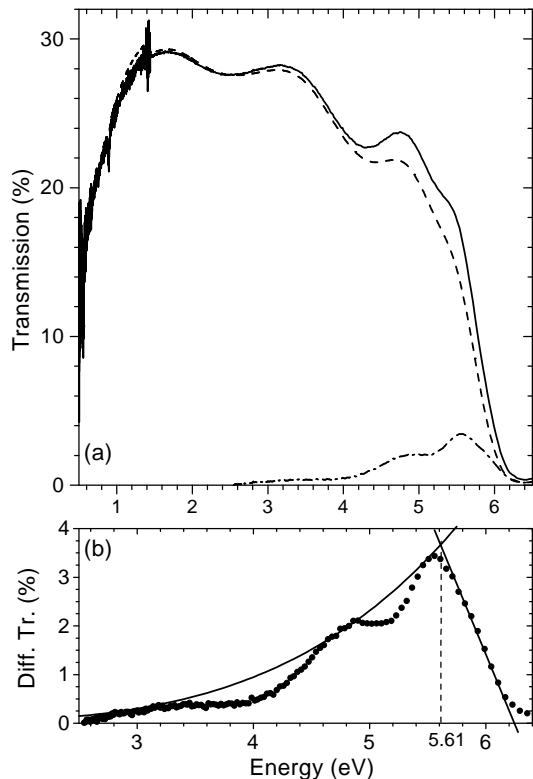


FIG. 6: (a) Total (solid line), specular (dashed line) and diffuse (dashed dotted line) transmission as a function of photon energy for a 150 nm thick  $\text{MgH}_2$  film capped with 12 nm Pd and loaded at  $100^\circ\text{C}$  in 100 bar of hydrogen. (b) Detail of the diffuse transmission. A fit using Eq. 2 and an extrapolation of the transmission edge are shown. The intersection of these two curves gives an estimate of 5.61 eV for the optical band gap.

and 10). The frequency dependence of  $\alpha$  near the band edge is related to the optical gap through,<sup>55,56</sup>

$$\alpha(\omega) \propto \frac{(\hbar\omega - E_g)^\nu}{\hbar\omega}. \quad (3)$$

For direct, allowed (forbidden) transitions  $\nu = \frac{1}{2}$  ( $\nu = \frac{3}{2}$ ) and for indirect, allowed (forbidden) transition  $\nu = 2$  ( $\nu = 3$ ). In amorphous material it has been found that  $\nu = 2$  gives the best results. Combining these equations gives

$$\ln T(\omega) = \ln T_0 - C \frac{(\hbar\omega - E_g)^\nu}{\hbar\omega}, \quad (4)$$

and the constants  $\ln T_0$ ,  $C$ , and  $E_g$  are determined from

a fit to the spectra near the transmission edge in the interference-free region.

Applied to the total transmission this 'Tauc procedure' gives a gap of  $5.48 \pm 0.05$  eV using  $\nu = 2$ . It was also possible to get a Tauc fit with  $\nu = 3$  and  $\nu = \frac{3}{2}$ . However, using  $\nu = 3$  gives values that are too low compared to the 'Rayleigh procedure' and we might be fitting an interference fringe instead of the absorption edge. For  $\nu = \frac{3}{2}$  the quality of the fit is not as good and we obtain a gap of  $5.75 \pm 0.05$  eV from the total transmission.

Since the diffuse transmission increases rapidly at small wavelengths (i.e. with increasing energy), it is clearer where the absorption starts in this spectrum than in the total transmission. Therefore, we conclude that the band gap of  $\text{MgH}_2$  is  $5.6 \pm 0.1$  eV.

## C. Ellipsometry

### 1. Modeling strategy

Extracting the dielectric function of a layer from ellipsometric data on samples like ours, which consists of several thin layers on a substrate, is a complex task. The complicated inversion of the ellipsometric data to the dielectric function is, however, greatly simplified if the optical properties of each individual layer is measured in separate experiments. For this reason we adopted the following strategy to determine the dielectric function of  $\text{MgH}_2$ .

We start by investigating the dielectric properties of the quartz substrate. The second step is to evaluate the optical properties of the hydrogenated Pd cap layer. This is done by investigating a 12 nm thick film of Pd on quartz, hydrogenate it in 1 bar  $\text{H}_2$  using the optical gas loading cell and measure it in the ellipsometer. In a third step we study the properties of the hydrogenated interface region between Pd and  $\text{MgH}_2$  carefully since earlier experiments with Mg-Pd thin films showed that interdiffusion starts already at  $100^\circ\text{C}$ .<sup>40,50</sup> This is done by investigating a 'Pd-Mg' alloy layer consisting of 10 nm Mg on a quartz substrate covered with 10 nm Pd. This sample is loaded with hydrogen at  $100^\circ\text{C}$  and 100 bar and measured in the ellipsometer. The final step is to measure the total stack (quartz,  $\text{MgH}_2$ , Pd-Mg) and to extract the optical properties of  $\text{MgH}_2$  using the optical properties of all the other layers.

An optical model is defined for each sample and in the fitting procedure the difference between the calculated (cal) and the measured (exp) ( $\Psi$ ,  $\Delta$ )-values (see Sec. II C) are weighted with the experimental standard deviation  $\sigma$  and fitted with a Levenberg-Marquardt algorithm to minimize the mean squared error (MSE) according to<sup>57,58</sup>

$$\text{MSE} = \frac{1}{2N - M} \sum_{\lambda} \sum_{\Theta} \left\{ \left[ \frac{\Psi_{\lambda, \Theta, \text{cal}} - \Psi_{\lambda, \Theta, \text{exp}}}{\sigma_{\lambda, \Theta, \Psi}} \right]^2 + \left[ \frac{\Delta_{\lambda, \Theta, \text{cal}} - \Delta_{\lambda, \Theta, \text{exp}}}{\sigma_{\lambda, \Theta, \Delta}} \right]^2 \right\} \quad (5)$$

where  $N$  is the number of  $(\Psi, \Delta)$ -pairs,  $M$  is the number of fitting parameters, and the indices  $\lambda$  and  $\Theta$  denote data points at different wavelengths and angles. In most cases also normal incidence transmission data,  $T$ , are used to improve the accuracy of the determination of the dielectric function.<sup>59</sup> Then, a third term is included in the summation in Eq. 5.

In the modeling we take into account experimental errors in incident angle and angular spread due to the substrate design, and film thickness non-uniformity. It is difficult to model both the thickness and the dielectric properties simultaneously in ellipsometry.<sup>46,47</sup> Thus, we allow the layer thicknesses to vary only slightly around our measured thickness values during fitting. The output from the modeling consists of the best-fit value of the Lorentz-Drude parameters (see Eq. 6) and their 90% confidence intervals.

## 2. Optical constants of the glass substrate

The optical constants of the quartz substrates (both flat and semi-cylindrical) and the quartz window used in the optical gas loading cell (see Fig. 2) are determined using optical reflection and transmission measurements and ellipsometry. This is straightforward, and our results match the tabulated values of the refractive index from the manufacturer as well as those of quartz glass cited in Ref. 60 (see Fig. 7(a)). The extinction coefficients being not tabulated in Ref. 60 are assumed to be zero. Our results on the extinction coefficient show a slight absorption near and above 6.5 eV, but still below  $10^{-7}$  (see Fig. 7(b)). The corresponding dielectric function is used in the consecutive modeling of the metal hydride layers.

## 3. Optical properties of $\text{PdH}_x$

A 12 nm thick Pd film, deposited on quartz is exposed to 1 bar hydrogen at RT in the optical gas loading cell and investigated in the ellipsometer (see Fig. 8 for the experimental and fitted data). The Pd hydride,  $\text{PdH}_x$ , that is formed is a strongly absorbing metal. Its dielectric function  $\epsilon(\omega) = \epsilon_1 + i\epsilon_2$  can be adequately parameterized with a Lorentz-Drude (LD) model:

$$\epsilon(\omega) = \epsilon_{\infty} - \sum_{i=1}^N \frac{\omega_{p,i}^2}{\omega^2 + i\omega/\tau_i} + \sum_{j=1}^M \frac{f_j}{\omega_j^2 - \omega^2 - i\Gamma_j\omega} \quad (6)$$

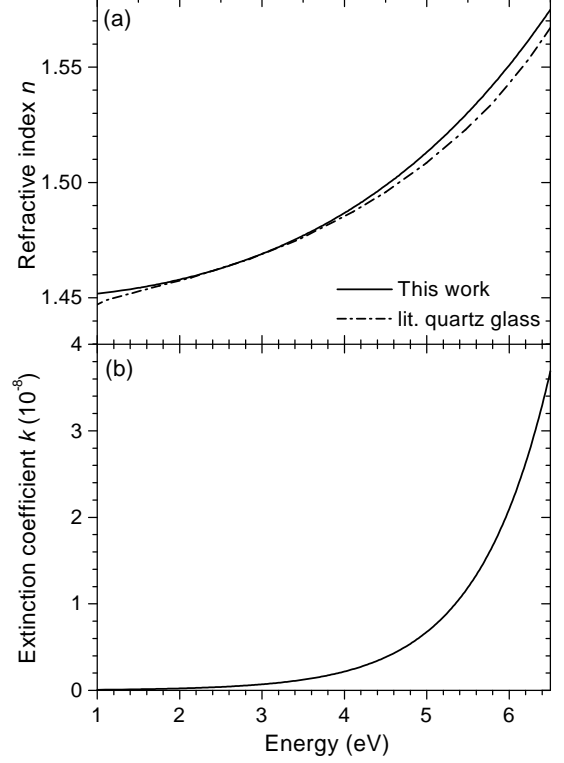


FIG. 7: (a) Refractive index,  $n$  and (b) extinction coefficient,  $k$  (b) of the quartz substrates as determined from ellipsometry and reflection and transmission measurements. For comparison literature data for the refractive index of quartz glass in Ref. 60 are shown as a dot-dashed line.

where the constant  $\epsilon_{\infty}$  accounts for excitations far above 6.5 eV; the  $N$  Drude terms describe the free-carrier response with  $\omega_{p,i}$  the plasma frequency of the  $i$ -th Drude term and  $\tau_i$  the relaxation time; the  $M$  Lorentz terms represent the effect of interband transitions with  $f_j$  the intensity of the  $j$ -th oscillator,  $\omega_j$  its energy, and  $\Gamma_j$  its broadening. The relation between the dielectric function and the refractive index,  $n$  and extinction coefficient,  $k$ , is:  $\epsilon_1 = n^2 - k^2$  and  $\epsilon_2 = 2nk$ . The LD parameters obtained for  $\text{PdH}_x$  in 1 bar  $\text{H}_2$  are given in Table I.

In addition to the sample for ellipsometry, an identical sample on a flat substrate is prepared for measurements in the spectrophotometer. The transmission and absolute reflection are determined for this sample in 40 mbar hydrogen (4%  $\text{H}_2$  in Ar). At higher pressures it is not

TABLE I: Lorentz-Drude parameters and their 90% confidence intervals of a 12 nm thick  $\text{PdH}_x$  layer in 1 bar  $\text{H}_2$  obtained from ellipsometric data (see Fig. 8).  $\text{MSE} = 7.4$ ,  $\epsilon_\infty = 1.266 \pm 0.371$ . All parameters are in eV.

$(i)$	$\omega_{p,i}$	$1/\tau_i$	$(j)$	$\omega_j$	$\sqrt{f_j}$	$\Gamma_j$
(1)	$3.389 \pm 0.901$	$0.1892 \pm 0.019$	(1)	$3.418 \pm 0.124$	$8.588 \pm 4.6$	$5.195 \pm 0.691$
(2)	$8.656 \pm 2.02$	$1.775 \pm 0.147$	(2)	$6.878 \pm 0.119$	$11.32 \pm 4.63$	$7.713 \pm 0.519$
			(3)	9.669	11.96	0.5601

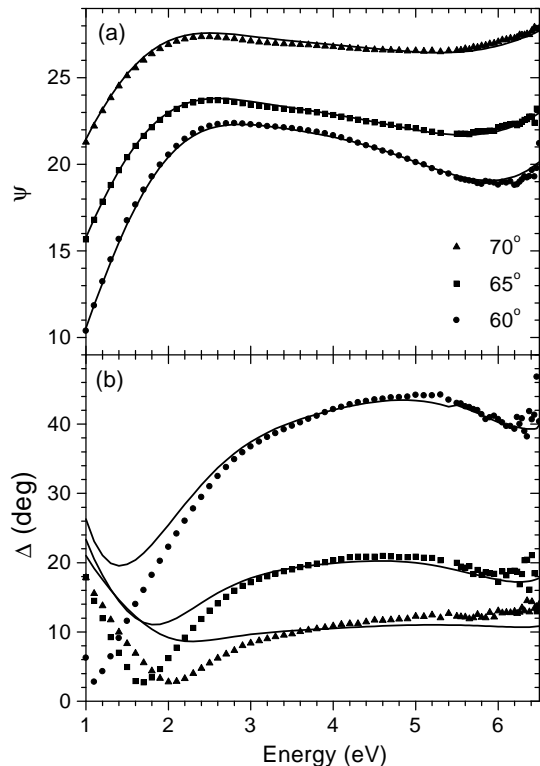


FIG. 8: Experimental and fitted ellipsometric data,  $\Psi$ , (a) and  $\Delta$  (b) for a 12 nm thick Pd film in 1 bar  $\text{H}_2$  used to determine the dielectric function of  $\text{PdH}_x$  (see Fig. 10). The mean square error corresponding to the fit is 7.4.

possible to use the optical gas loading cell when we determine the absolute reflection since we must look directly at the Pd sample and not via the substrate. To obtain a hydrogenated Pd sample, the whole spectrophotometer is purged in Ar containing 4%  $\text{H}_2$ , corresponding to a partial pressure of 40 mbar  $\text{H}_2$ . This is the highest  $\text{H}_2$  concentration we can use in the (open) spectrophotometer. In Fig. 9 the experimental and fitted data are displayed, the LD parameters obtained for  $\text{PdH}_x$  in 40 mbar  $\text{H}_2$  are given in Table II.

The difference in the MSE (see Table I and II) between

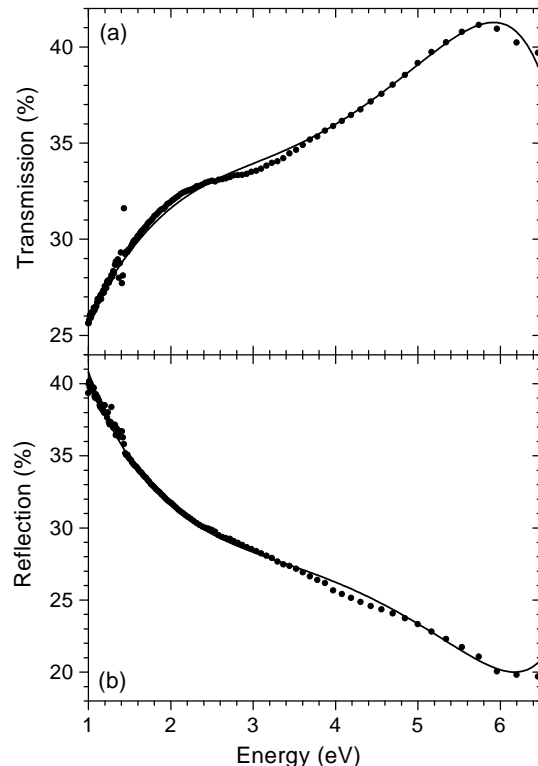


FIG. 9: Experimental and fitted transmission (a) and reflection (b) data for a 12 nm thick Pd film in 40 mbar  $\text{H}_2$  (4% H in Ar) used to determine the dielectric function of  $\text{PdH}_x$  (see Fig. 10). The mean square error corresponding to the fit is 1.04.

the 1 bar and 40 mbar measurements is mainly due to the different substrate geometry, semi-cylindrical vs. flat substrate. We assign the major part of the difference in the MSE to the cylindrical incident and exit surface of the semi-cylindrical substrate and to the fact that the ellipsometry measurements have been performed from the ‘backside’ of the sample through the substrate. Note that this does not change the dielectric function, it merely gives a larger spread in the input data for the analysis.

In Fig. 10 we show the resulting dielectric function at



TABLE II: Lorentz-Drude parameters and their 90% confidence intervals of a 12 nm thick  $\text{PdH}_x$  layer in 40 mbar  $\text{H}_2$  (4%  $\text{H}_2$  in Ar) obtained from reflection and transmission data (see Fig. 9).  $\text{MSE} = 1.04$ ,  $\epsilon_\infty = 1.280 \pm 0.241$ . All parameters are in eV.

(i)	$\omega_{p,i}$	$1/\tau_i$	(j)	$\omega_j$	$\sqrt{f_j}$	$\Gamma_j$
(1)	$5.156 \pm 0.955$	$0.001 \pm 0.0241$				
(2)	$8.382 \pm 2.65$	$2.238 \pm 0.323$				
			(1)	$4.131 \pm 0.111$	$9.815 \pm 4.17$	$7.104 \pm 0.581$
			(2)	$7.623 \pm 0.249$	$7.793 \pm 4.14$	$0.927 \pm 0.235$

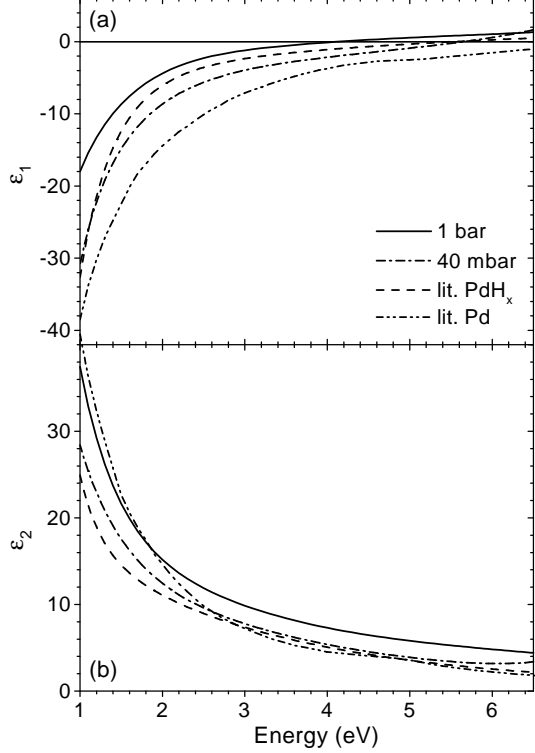


FIG. 10: Real (a) and imaginary (b) parts of  $\epsilon(\omega)$  for the  $\text{PdH}_x$  films as determined from ellipsometry in 1 bar  $\text{H}_2$  (see Fig. 8) and reflection and transmission measurements in 40 mbar  $\text{H}_2$  (4%  $\text{H}_2$  in Ar) (see Fig. 9). For comparison, the dielectric function found by Rottkay *et al.*<sup>61</sup> for  $\text{PdH}_x$  in 4%  $\text{H}_2$  and the dielectric function of pure Pd according to Ref. 60 are included.

1 bar, and 40 mbar  $\text{H}_2$  partial hydrogen pressure, and compare it to literature data for  $\text{PdH}_x$  by Rottkay *et al.*<sup>61</sup> and literature data for Pd from Ref. 60.

The plasma frequency,  $\omega_p$ , of  $\text{PdH}_x$  in 1 bar  $\text{H}_2$  is slightly larger than the one in 40 mbar  $\text{H}_2$ . Because  $\omega_p \propto \sqrt{n_c}$  with  $n_c$  the charge carrier density, there are more free charge carriers in  $\text{PdH}_x$  in 1 bar than in 40 mbar  $\text{H}_2$ . Values for the (optical) resistivity  $\rho$  can be

derived from the Drude parameters using

$$\rho_{\text{opt}} = \frac{1}{\epsilon_0 \omega_p^2 \tau}, \quad (7)$$

with  $\epsilon_0$  the vacuum permittivity,  $\omega_p$  the plasma frequency and  $\tau$  the electron relaxation time. This optical resistivity calculated for the dominant Drude term no. 2 shows the same trend as the plasma frequency itself: In 40 mbar  $\text{H}_2$   $\text{PdH}_x$  has a resistivity of  $235 \mu\Omega\text{cm}$ , in 1 bar  $178 \mu\Omega\text{cm}$ . However, bulk Pd has a resistivity of  $10.53 \mu\Omega\text{cm}$  and  $\text{PdH}_x$  has a maximum resistivity of about  $20 \mu\Omega\text{cm}$  when  $x = 0.7$  at RT.<sup>62</sup> Our much larger resistivities are probably due to the fact that the 12 nm thick Pd film consists of somewhat disconnected islands. Hydrogen absorption causes the Pd islands to expand which decreases the resistivity between them.<sup>63,64</sup> Thus, we have a sort of percolation effect and the resistivity is lower in 1 bar  $\text{H}_2$  than in 40 mbar  $\text{H}_2$  contrary to bulk  $\text{PdH}_x$ .

#### 4. Optical constants of the double layer Pd/Mg

To investigate the optical properties of the partially interdiffused Pd-Mg top layer, we deposit a layer of 10 nm Mg capped with 10 nm Pd on quartz. This Pd-Mg film is then exposed to hydrogen at  $100^\circ\text{C}$  and 100 bar (together with the thick Mg film covered by Pd (see Fig. 1)). After hydrogenation the optical properties are determined in the optical gas loading cell at RT. This sample is treated as consisting of two layers: a Mg-rich Pd-Mg alloy on the substrate covered with a Pd-rich Pd-Mg alloy on top. As starting values for the fitting procedure we use the  $\text{PdH}_x$  dielectric function determined above for the Pd-rich Pd-Mg top layer, and combine it with voids in a Bruggeman effective medium approximation (EMA) to take surface roughness into account.<sup>65</sup> A Lorentz-Drude model is used for the second layer, the Mg-rich Pd-Mg alloy. Ellipsometric data for three angles of incidence ( $55^\circ$ ,  $60^\circ$  and  $65^\circ$ ) and normal incidence transmission data are then combined in a multiple data type fit. All data are measured on the same sample and during fitting the layer optical functions and thicknesses are coupled. The final iteration results in a fit with a MSE of 8.7. The optical properties of this double layer are then used as starting values for the top layer of the thicker  $\text{MgH}_2$  film.

### 5. Dielectric function of $\text{MgH}_2$

In the evaluation of the optical properties of  $\text{MgH}_2$  we analyze ellipsometric and transmission data of a 124 nm thick  $\text{MgH}_2$  film capped with 12 nm  $\text{PdH}_x$  (as measured with a mechanical stylus profilometer in the hydrogenated state). In addition to these data, transmission data of a compositionally identical film, but with a thickness of 162 nm (when hydrogenated) are included in the modeling. These three data sets are evaluated in three parallel, coupled models simultaneously. The main features can be modeled using two Lorentz oscillators at the high energy side of the measured spectra, at 6.4 and 6.9 eV. These oscillators mark the beginning of the conduction band.

The optical parameters of the capping layer, consisting of the Pd-rich Pd-Mg alloy on top of the Mg-rich Pd-Mg alloy, are initially fixed to the parameter values obtained in Section III C 4. The only parameters of the top layers which are allowed to vary are the thicknesses since the diffusion of Pd into  $\text{MgH}_2$  may be larger than the 10 nm in the thin Pd/Mg double layer. In the final iteration a global fit is used in which all LD parameters are allowed to change. The final MSE is 17.17. Table III gives the LD parameter values from the final iteration for  $\text{MgH}_2$ , the Pd-rich Pd-Mg cap layer and the Mg-rich Pd-Mg cap layer.

The plasma frequencies obtained for the two top layers give us a clue about their composition. Since the plasma frequency of the top layer ( $\omega_p = 14.35$  eV) is much larger than the one of the lower cap layer ( $\omega_p = 6.672$  eV), the top layer has a larger charge carrier density and is thus more metallic than the lower one. This indicates that the top layer is formed by a *metallic* Pd-Mg alloy. The lower layer contains some insulating  $\text{MgH}_2$  as well. The optical resistivity (see Eq. 7) of the top layer is  $38 \mu\Omega\text{cm}$  compared to an electrical resistivity of  $63 \mu\Omega\text{cm}$  (at RT) for the total stack as measured after loading. Thus, the top layer is indeed shunting the resistivity measurements of  $\text{MgH}_2$ . Since  $\text{PdH}_x$  has an optical resistivity of  $178 \mu\Omega\text{cm}$  it is clear that the top layer contains some metallic Mg as well which has a much lower resistivity ( $6.5 \mu\Omega\text{cm}$ ).

The total thickness of the stack obtained from ellipsometry is 130.6 nm after hydrogenation. With the stylus profilometer we found a thickness of 136 nm. However, as mentioned before the profilometer gives a value that is too large. Before hydrogenation the thickness was 95 nm. This would mean an increase of 37.5% instead of the theoretical 32% volume expansion.

In Fig. 11(a),(b) the experimental and fitted values of  $\Psi$  and  $\Delta$  are given, in (c),(d) the experimental and fitted transmission curves are shown. Finally, Fig. 12(a),(b) shows the real and imaginary part of  $\epsilon(\omega)$  obtained for  $\alpha\text{-MgH}_2$ .

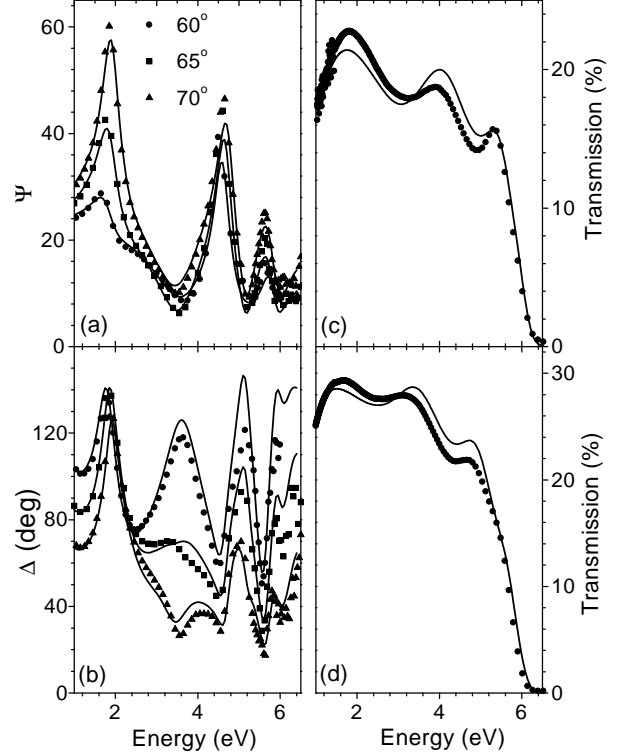


FIG. 11: Experimental and fitted data for a 124 nm thick  $\text{MgH}_2$  film covered with 12 nm Pd used to determine the dielectric function of  $\text{MgH}_2$  (see Fig. 12); (a) ellipsometric data for  $\Psi$ , (b) ellipsometric data for  $\Delta$ , (c) optical transmission (d) transmission of a sample consisting of 150 nm  $\text{MgH}_2$ /12 nm Pd. All experimental data are modelled simultaneously in the fitting procedure as described in Sec. III C. The mean square error of the fit is 17.17.

## IV. DISCUSSION

In Table IV both experimental and theoretical values for the band gap of  $\text{MgH}_2$  are given. Hartree-Fock (HF) calculations are not included since this method overestimates the band gap considerably. Very recent and not yet published theoretical work by Herzig<sup>66</sup>, Auluck<sup>67</sup> and Alford and Chou<sup>1</sup> on  $\text{MgH}_2$  is included.

The band gap of  $5.6 \pm 0.1$  eV determined in this work for  $\alpha\text{-MgH}_2$  is close to values mentioned sporadically in literature. The value 5.16 eV was obtained in an UV-absorption study mentioned by Krasko.<sup>15</sup> However, details about how this value was obtained have never been published. The value found by He and Pong<sup>16</sup> for the average band gap  $\langle E_g \rangle$  is close to ours. This is rather surprising since  $\langle E_g \rangle$  was obtained in an indirect way from X-ray photoelectron spectroscopy (XPS) data using Penn's formula.<sup>17</sup> Yamamoto *et al.*<sup>18</sup> measured the specular optical transmission of thin layers of  $\text{MgH}_2$  cov-

TABLE III: Lorentz-Drude parameters and their 90% confidence intervals of a 124 nm MgH<sub>2</sub> film covered with 12 nm Pd obtained from ellipsometric and transmission data (see Fig. 11). MSE = 17.17 and  $\epsilon_\infty = 1.595 \pm 0.092$ . All parameters are in eV.

MgH <sub>2</sub> film, $d = 115.9$ nm						
$(i)$	$\omega_{p,i}$	$1/\tau_i$	$(j)$	$\omega_j$	$\sqrt{f_j}$	$\Gamma_j$
			(1)	6.4	5.516	0.6454
			(2)	6.9	$7.689 \pm 0.519$	$0.01223 \pm 0.109$
Top cap layer: Pd-rich Pd-Mg alloy (with 53% voids), $d = 15.6$ nm						
$(i)$	$\omega_{p,i}$	$1/\tau_i$	$(j)$	$\omega_j$	$\sqrt{f_j}$	$\Gamma_j$
(1)	$14.35 \pm 0.062$	$1.055 \pm 30.6$	(1)	$2.964 \pm 0.122$	$5.208 \pm 0.559$	$1.702 \pm 9.03$
			(2)	8.5	$17.408 \pm 12.2$	$0.01366 \pm 4.96$
Lower cap layer: Mg-rich Pd-Mg alloy, $d = 4.1$ nm						
$(i)$	$\omega_{p,i}$	$1/\tau_i$	$(j)$	$\omega_j$	$\sqrt{f_j}$	$\Gamma_j$
(1)	$6.672 \pm 0.865$	$0.003629 \pm 8.29$	(1)	$3.293 \pm 0.0824$	$24.61 \pm 0.420$	$14.09 \pm 7.06$

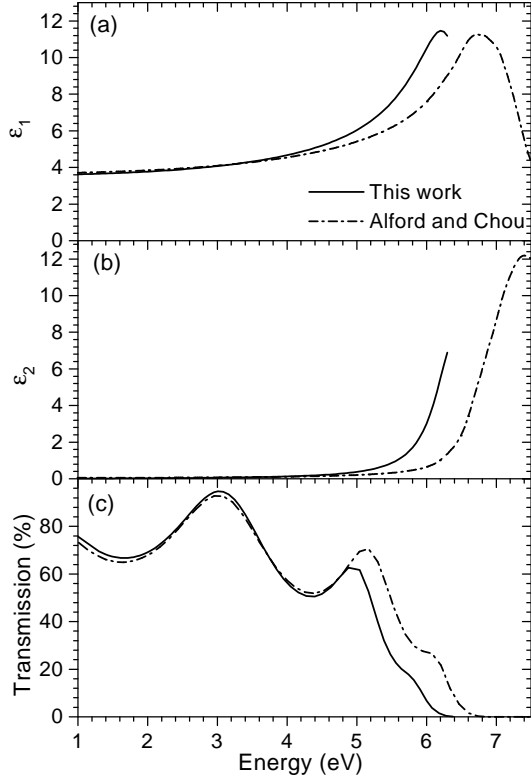


FIG. 12: Real (a) and imaginary (b) parts of  $\epsilon(\omega)$  for MgH<sub>2</sub> determined from ellipsometry and transmission data (see Fig. 11). The real and imaginary parts calculated by Alford and Chou<sup>1</sup> using the GW approximation are shown for comparison. The transmission of a 100 nm MgH<sub>2</sub> film in vacuum calculated with the dielectric functions shown in (a) and (b) is displayed in the lower panel (c). The theoretical gap is approximately 0.5 eV too large.

TABLE IV: Literature data for the band gap,  $E_g$ , of MgH<sub>2</sub> both experimental (expt.) and calculated (calc.). In parentheses the smallest direct gap for MgH<sub>2</sub> is given.

Material		Method	$E_g$ (eV)	Ref.
$\alpha$ -MgH <sub>2</sub>	expt.	UV-absorption	5.16	15
		XPS	5.8	16
		EELS	$>3.7^a$	68
		XPS	$>3.4^a$	69
		Transmission	$6.05^b$	18
	calc.	Ellipsometry/Transmission	$5.6 \pm 0.1$	this work
		LDA	3.06	12
		LDA	3.4	13
		LDA	3.45 (4.34)	66
		LDA	3.3	67
$\gamma$ -MgH <sub>2</sub>	calc.	LDA	3.10	1
		GGA	3.78	14
		GGA	4.2	9
		sX-LDA	5.71 (6.41)	66
$\beta$ -MgH <sub>2</sub>	calc.	GWA	5.25 (6.11)	1
		GGA	4.3	9
		APW	0.23	70
		GGA	2.35	71

<sup>a</sup>If there are no charging effects, the band gap would be twice the indicated value.

<sup>b</sup>This is the photon energy where the transmission vanishes.

ered by Pd and found that the transmission is zero at 6.05 eV. However, they did not apply Tauc's method (see Sec. III B) to the transmission edge in order to obtain an estimate for the band gap. Furthermore, one should keep in mind that 6.02 eV is at the detection limit of their Shimadzu spectrophotometer.

As can be seen in Table IV LDA calculations give a band gap that is systematically too low. This is a well-known feature of this approximation. Similarly, the GGA used in two other papers<sup>9,14</sup> to calculate the density of states of  $\text{MgH}_2$ , underestimates the band gap. Our band gap is closest to the theoretically calculated gaps of Herzig<sup>66</sup> using screened-exchange-LDA (sX-LDA) and Alford and Chou<sup>1</sup> using the GW approximation (GWA). Furthermore, it is interesting to point out that our experimentally found gap  $E_g = 5.6 \pm 0.1$  eV is very close to the difference in ionization energy between Mg and H: 5.952 eV.

Back in 1955 Ellinger *et al.*<sup>19</sup> determined the refractive index of  $\alpha\text{-MgH}_2$  at 589.3 nm (2.107 eV) and found  $n = 1.95$  and  $1.96$  for the ordinary and extraordinary rays, respectively. We find  $n = 1.94$  and  $k = 7.6 \cdot 10^{-3}$  at the same energy which is very close.

Both Auluck<sup>67</sup> using LDA and Alford and Chou<sup>1</sup> using LDA and GWA have calculated the band structure and dielectric function for  $\alpha\text{-MgH}_2$ . To obtain the dielectric function only direct transitions are taken into account. The only difference between the LDA and GWA curves is the energy position. The dielectric function obtained for  $\alpha\text{-MgH}_2$  with GWA agrees quite well with our measured values (see Fig. 12 (a),(b)), while the LDA curve, as expected, is shifted to too low energies. This indicates that a scissors-operation that shifts the conduction band rigidly with respect to the valence band works well to correct LDA calculations.<sup>72,73</sup> The energy at which both  $\epsilon_1$  and  $\epsilon_2$  exhibit a marked increase is, however, slightly different for the experiment and the GWA calculation. sX-LDA seems to overestimate the band gap since it gives even larger values for the (in)direct gap than GWA.

Figure 12(c) shows the optical transmission for a 100 nm thick  $\text{MgH}_2$  film in vacuum as calculated with our experimental dielectric function and the one calculated by Alford and Chou. As can be seen  $\text{MgH}_2$  has an intrinsic transparency of about 80% over the entire visible spectrum. The difference in energy between the absorption edges of the two transmission spectra and the dielectric functions is about 0.5 eV. Thus, GWA overestimates the optical gap by 0.5 eV. The direct gap determined from the band structure using GWA is 6.11 eV. Subtracting 0.5 eV from 6.11 eV gives a value of 5.61 eV which is within the error margin of our experimentally found gap. More information about the dielectric function and band structure of  $\text{MgH}_2$  by Alford and Chou will be published elsewhere.

Yet unpublished calculations indicate that the optical properties of both  $\alpha$ - and  $\gamma$ - $\text{MgH}_2$  are close to each other.<sup>1,67</sup> Vajeeston *et al.*<sup>9</sup> find a gap of 4.2 and 4.3 eV for  $\alpha$ - and  $\gamma$ - $\text{MgH}_2$ , respectively with GGA; Bastide *et al.*<sup>10</sup> and Bortz *et al.*<sup>11</sup> have found that the structures of the two different phases are closely related and that the density is almost the same as well as the H-H distances. Therefore, our dielectric function for  $\alpha\text{-MgH}_2$  is probably a very good approximation for  $\gamma\text{-MgH}_2$  as well. This is important to model the optical properties of switchable

TABLE V: Literature data for the band gap,  $E_g$ , of materials closely related to  $\text{MgH}_2$  both experimental (expt.) and calculated (calc.).

Material		Method	$E_g$ (eV)	Ref.
$\text{MgF}_2$	expt.	Reflectance	12.4	74
	calc.	tight-binding, pseudopotentials	12.8	75
$\text{MgO}$	expt.	Reflectance	7.77	76
	calc.	LDA	$\sim 5$	77
		GWA	7.8	77,78
$\text{MgS}$	calc.	LDA	2.6	79
		LDA (corrected)	4.59	80
$\text{MgSe}$	expt.		5.6	81
$\text{MgTe}$	expt.		4.7, 3.6	81
$\text{CaH}_2$	expt.	XPS	$\sim 5^a$	82
		SRPES	$\sim 5^a$	83
	calc.	LDA	3.32	84
$\text{SrH}_2$	expt.	XPS	$\sim 5^a$	82
$\text{BaH}_2$	expt.	XPS	$\sim 5^a$	82
		XPS	$> 2.2^b$	69
$\text{LiH}$	expt.		4.99	85
	calc.	GWA	5.24	85
$\text{LiD}$	expt.		5.04	78
	calc.	LDA	2.84	78
		GWA	5.37	78

<sup>a</sup>Charging effects are taking into account in the experiments.

<sup>b</sup>If there are no charging effects, the band gap would be twice as large.

mirrors since in fully hydrogenated Y-Mg alloys Nagengast *et al.* found that fcc  $\text{YH}_3$  coexists with  $\gamma\text{-MgH}_2$ .<sup>28</sup>  $\beta\text{-MgH}_2$  seems to be very different both structurally<sup>10</sup> and optically. Its density is much larger and the calculated band gap for this material turns out to be considerably smaller than that of both  $\alpha$ - and  $\gamma\text{-MgH}_2$  (see Table IV). The augmented plane wave (APW) calculations underestimate the band gap considerably, the GGA value of 2.35 eV (again by Vajeeston<sup>71</sup>) is much more reliable. The difference between the calculated band gap using GGA and the one measured for  $\alpha\text{-MgH}_2$  is 1.4 eV. Assuming that the same scissors-operation can be applied we expect an experimental gap of 5.7 eV for  $\gamma\text{-MgH}_2$  and 3.75 eV for  $\beta\text{-MgH}_2$ .

We now compare  $\text{MgH}_2$  to related materials such as  $\text{MgF}_2$ ,  $\text{MgO}$ ,  $\text{MgS}$ ,  $\text{MgSe}$ , and other alkaline-earth and alkali hydrides. In Table V the band gaps of these materials are listed. For all of them it turns out that LDA underestimates the measured gap. Again, as for  $\text{MgH}_2$ , the GW approximation seems to give a very good agreement between experiment and calculation for  $\text{MgO}$ ,  $\text{LiH}$  and  $\text{LiD}$ . The same is true for the alkali halides.<sup>78</sup>  $\text{MgH}_2$  and  $\text{CaH}_2$  seem to be very similar. Both materials are wide band gap insulators and have a valence band that

is predominantly determined by hydrogen orbitals.<sup>12,13,84</sup> For MgO and MgS both valence and conduction bands are determined by the anions (O or S)<sup>79</sup> as well and again the same holds for the alkali halides.<sup>86</sup>

Since both the valence and conduction band of MgH<sub>2</sub> are formed by H states, the band gap of the alkaline-earth hydrides is expected to be almost independent of the metal as is the case for the alkali halides.<sup>86,87</sup> The remaining dependence results from the influence of the metal-ion on the lattice parameter, and the influence of hybridization of the conduction band states with metal-ion *s*- and *d*-states. From XPS experiments by Franzen *et al.*<sup>82</sup> it seems that the onset of transitions in the valence band regions start for CaH<sub>2</sub>, SrH<sub>2</sub> and BaH<sub>2</sub> all at about 2.5 eV. Since charging effects are taken into account, this gives a gap of about 5 eV quite close to what we have found for  $\alpha$ -MgH<sub>2</sub>. It is striking that LiH and LiD also have a gap of 5.0 eV.

## V. CONCLUSIONS

In this study we use a novel experimental setup for optical transmission and ellipsometry measurements. This setup facilitates greatly measurements of the optical properties and dielectric function of metal hydrides in a hydrogen environment. It is possible to control the gas pressure from 1 mbar to 100 bar, and thus the composition of metal hydrides over a wide range. The temperature, pressure and resistivity are monitored *in situ* during hydrogenation of a sample. We determine the dielectric properties of  $\alpha$ -MgH<sub>2</sub> and PdH<sub>x</sub> and find that MgH<sub>2</sub> is a transparent, colour neutral insulator with a band gap

of  $5.6 \pm 0.1$  eV. The transparency over the whole visible spectrum is  $\sim 80\%$  (for a 100 nm thick film). The experimentally determined dielectric function in the photon energy range between 1 and 6.5 eV of  $\alpha$ -MgH<sub>2</sub> is in very good agreement with very recent calculations using the GW approximation. If we assume that calculations of the band gap for  $\gamma$ - and  $\beta$ -MgH<sub>2</sub> underestimate the experimental gap by the same amount as in  $\alpha$ -MgH<sub>2</sub> we expect an experimental gap of 5.7 eV for  $\gamma$ -MgH<sub>2</sub> and 3.75 eV for  $\beta$ -MgH<sub>2</sub>.

In a coming publication we shall show that the dielectric function of MgH<sub>2</sub> determined here can be used to explain the large optical absorption (the so-called ‘black state’) of Mg-based alloys where metallic Mg and insulating MgH<sub>2</sub> nanodomains coexist.

## Acknowledgments

The authors would like to thank N.J. Koeman, J.H. Rector and W. Lohstroh for their valuable help with the deposition and characterization of the samples. L. Jansen is gratefully acknowledged for constructing the optical gas loading cell and high pressure loading chamber. We are also very grateful to J.A. Alford, M.Y. Chou, P. Herzig, S. Auluck and P. Vajeeston for making available to us the results of their band structure calculations before publication. This work is part of the research program of the Stichting voor Fundamenteel Onderzoek der Materie (FOM), financially supported by the Nederlandse Organisatie voor Wetenschappelijk Onderzoek (NWO).

---

\* Present address: Solid State Physics, Uppsala University, Box 534, SE-751 21 Uppsala, Sweden

† Corresponding author. Electronic address: giebels@nat.vu.nl

<sup>1</sup> J. A. Alford and M. Y. Chou, (unpublished).

<sup>2</sup> H. Kohlmann (Academic Press, New York, 2002), vol. 9 of *Encyclopedia of physical sciences and technology*, chap. Metal Hydrides, 3rd ed.

<sup>3</sup> L. Schlapbach and A. Züttel, *Nature* **414**, 353 (2001).

<sup>4</sup> P. Selvam, B. Viswanathan, C. S. Swamy, and V. Srinivasan, *Int. J. Hydrogen Energy* **11**, 169 (1986).

<sup>5</sup> A. Zaluska, L. Zaluski, and J. O. Ström-Olsen, *J. Alloys Compd.* **288**, 217 (1999).

<sup>6</sup> G. Liang, J. Huot, S. Boily, A. Van Neste, and R. Schulz, *J. Alloys Compd.* **292**, 247 (1999).

<sup>7</sup> Z. Dehouche, R. Djazandry, J. Huot, S. Boily, J. Goyette, T. K. Bose, and R. Schulz, *J. Alloys Compd.* **305**, 264 (2000).

<sup>8</sup> J. F. Pelletier, J. Huot, M. Sutton, R. Schulz, A. R. Sandy, L. B. Lurio, and S. G. J. Mochrie, *Phys. Rev. B* **63**, 052103 (2001).

<sup>9</sup> P. Vajeeston, P. Ravindran, A. Kjekshus, and H. Fjellvåg, *Phys. Rev. Lett.* **89**, 175506 (2002).

<sup>10</sup> J. P. Bastide, B. Bonnetot, J. M. L  toff  , and P. Claudy, *Mat. Res. Bull.* **15**, 1215 (1980).

<sup>11</sup> M. Bortz, B. Bertheville, G. B  ttger, and K. Yvon, *J. Alloys Compd.* **287**, L4 (1999).

<sup>12</sup> R. Yu and P. K. Lam, *Phys. Rev. B* **37**, 8730 (1988).

<sup>13</sup> B. Pfrommer, C. Els  sser, and M. F  hnle, *Phys. Rev. B* **50**, 5089 (1994).

<sup>14</sup> U. H  ussermann, H. Blomqvist, and D. Nor  us, *Inorg. Chem.* **41**, 3684 (2002).

<sup>15</sup> G. Krasko, *Metal-Hydrogen Systems* (Pergamon, New York, 1982), p. 367.

<sup>16</sup> Z. X. He and W. Pong, *Physica Scripta* **41**, 930 (1990).

<sup>17</sup> D. R. Penn, *Phys. Rev.* **128**, 2093 (1962).

<sup>18</sup> K. Yamamoto, K. Higuchi, H. Kajioka, H. Sumida, S. Orimo, and H. Fujii, *J. Alloys Compd.* **330-332**, 352 (2002).

<sup>19</sup> F. H. Ellinger, J. C. E. Holley, B. B. McInteer, D. Pavone, R. M. Potter, E. Staritzky, and W. H. Zachariasen, *J. Am. Chem. Soc.* **77**, 2647 (1955).

<sup>20</sup> J. N. Huiberts, R. Griessen, J. H. Rector, R. J. Wijngaarden, J. P. Dekker, D. G. de Groot, and N. J. Koeman, *Nature* **380**, 231 (1996).

<sup>21</sup> P. H. L. Notten, M. Kremers, and R. Griessen, *J. Elec-*

- trochem. Soc. **143**, 3348 (1996).
- 22 E. S. Kooij, A. T. M. van Gogh, and R. Griessen, J. Electrochem. Soc. **146**, 2990 (1999).
  - 23 P. van der Sluis, M. Ouwerkerk, and P. A. Duine, Appl. Phys. Lett. **70**, 3356 (1997).
  - 24 T. J. Richardson, J. L. Slack, R. D. Armitage, R. Kostecki, B. Farangis, and M. D. Rubin, Appl. Phys. Lett. **78**, 3047 (2001).
  - 25 J. Isidorsson, I. A. M. E. Giebels, E. S. Kooij, N. J. Koeman, J. H. Rector, A. T. M. van Gogh, and R. Griessen, Electrochim. Acta **46**, 2179 (2001).
  - 26 S. J. van der Molen, D. G. Nagengast, A. T. M. van Gogh, J. Kalkman, E. S. Kooij, J. H. Rector, and R. Griessen, Phys. Rev. B **63**, 235116 (2001).
  - 27 J. Isidorsson, I. A. M. E. Giebels, M. Di Vece, and R. Griessen, SPIE Proc. **4458**, 128 (2001).
  - 28 D. G. Nagengast, A. T. M. van Gogh, E. S. Kooij, B. Dam, and R. Griessen, Appl. Phys. Lett. **75**, 2050 (1999).
  - 29 M. Di Vece, S. J. M. Zevenhuizen, and J. J. Kelly, Appl. Phys. Lett. **81**, 1213 (2002).
  - 30 M. Di Vece, A. M. J. van der Eerden, J. A. van Bokhoven, S. Lemaux, J. J. Kelly, and D. C. Koningsberger, Phys. Rev. B **67**, 035430 (2003).
  - 31 B. Darriet, M. Pezat, A. Hbika, and P. Hagenmuller, Int. J. Hydrogen Energy **5**, 173 (1980).
  - 32 D. Sun, F. Gingl, Y. Nakamura, H. Enoki, M. Bououdina, and E. Akiba, J. Alloys Compd. **333**, 103 (2002).
  - 33 I. A. M. E. Giebels, J. Isidorsson, E. S. Kooij, A. Remhof, N. J. Koeman, J. H. Rector, A. T. M. van Gogh, and R. Griessen, J. Alloys Compd. **330-332**, 875 (2002).
  - 34 R. Griessen, Phys. Bl. **53**, 1207 (1997).
  - 35 I. A. M. E. Giebels, J. Isidorsson, and R. Griessen, (unpublished).
  - 36 J. Isidorsson, I. A. M. E. Giebels, R. Griessen, and M. Di Vece, Appl. Phys. Lett. **80**, 2305 (2002).
  - 37 A. Krozer and B. Kasemo, J. Vac. Sci. Technol. A **5**, 1003 (1987).
  - 38 A. Krozer and B. Kasemo, J. Phys.: Condens. Matter **1**, 1533 (1989).
  - 39 J. Rydén, B. Hjörvarsson, T. Ericsson, E. Karlsson, A. Krozer, and B. Kasemo, J. Less-Common Met. **152**, 295 (1989).
  - 40 A. Krozer and B. Kasemo, J. Less-Common Met. **160**, 323 (1990).
  - 41 P. Spatz, H. A. Aebischer, A. Krozer, and L. Schlapbach, Z. Phys. Chem. **181**, 393 (1993).
  - 42 Z. Luz, J. Genossar, and P. S. Rudman, J. Less-Common Met. **73**, 113 (1980).
  - 43 R. J. Westerwaal, I. A. M. E. Giebels, N. J. Koeman, and R. Griessen, (unpublished).
  - 44 L. J. van der Pauw, Philips Res. Rep. **13**, 1 (1958).
  - 45 R. M. A. Azzam and N. M. Bashara, *Ellipsometry and polarized light* (North-Holland, Amsterdam, 1977).
  - 46 W. A. McGahan, B. Johs, and J. A. Woollam, Thin Solid Films **234**, 443 (1993).
  - 47 K. Järrendahl and H. Arwin, Thin Solid Films **313-314**, 114 (1998).
  - 48 P. Hjort, A. Krozer, and B. Kasemo, J. Alloys Compd. **234**, L11 (1996).
  - 49 D. R. Lide, ed., *Handbook of Chemistry and Physics* (CRC Press, Cleveland, 2001), 82nd ed.
  - 50 A. Fischer, H. Köstler, and L. Schlapbach, J. Less-Common Met. **172-174**, 808 (1991).
  - 51 S. J. van der Molen, J. W. J. Kerssemakers, J. H. Rector, N. J. Koeman, B. Dam, and R. Griessen, J. Appl. Phys. **86**, 6107 (1999).
  - 52 A. Borgschulte, M. Rode, A. Jacob, and J. Schoenes, J. Appl. Phys. **90**, 1147 (2001).
  - 53 T. Schober, Met. Trans. A **12A**, 951 (1981).
  - 54 Lord Rayleigh, Phil. Mag. **XLI**, 274 (1871).
  - 55 J. Tauc, R. Grigorovici, and A. Vancu, Phys. Stat. Sol. **15**, 627 (1966).
  - 56 E. J. Johnson, *Absorption near the fundamental edge* (Academic Press, New York, 1967), vol. 3 Optical properties of III-V compounds of *Semiconductors and semimetals*, chap. 6.
  - 57 G. E. Jr. Jellison, Appl. Opt. **30**, 3354 (1991).
  - 58 W. H. Press, B. P. Flannery, S. A. Teukosky, and W. T. Vetterling, *Numerical recipes: the art of scientific computing* (Cambridge University Press, Cambridge MA, 1988).
  - 59 B. D. Johs, W. A. McGahan, and J. A. Woollam, Thin Solid Films **253**, 25 (1994).
  - 60 E. D. Palik, ed., *Handbook of optical constants of solids* (Academic Press, San Diego, 1998).
  - 61 K. von Rottkay, M. Rubin, and P. A. Duine, J. Appl. Phys. **85**, 408 (1999).
  - 62 B. M. Geerken and R. Griessen, J. Phys. F: Met. Phys. **13**, 963 (1983).
  - 63 F. Favier, E. C. Walter, M. P. Zach, T. Benter, and R. M. Penner, Science **293**, 2227 (2001).
  - 64 O. Dankert and A. Pundt, Appl. Phys. Lett. **81**, 1618 (2002).
  - 65 D. E. Aspnes, J. B. Theeten, and F. Hottier, Phys. Rev. B **20**, 3292 (1979).
  - 66 P. Herzig, (private communication).
  - 67 S. Auluck, (private communication).
  - 68 P. T. Sprunger and E. W. Plummer, Chem. Phys. Lett. **187**, 559 (1991).
  - 69 A. Krozer, A. Fischer, and L. Schlapbach, Phys. Rev. B **53**, 13808 (1996).
  - 70 M. Gupta, Z. Phys. Chem. **181**, 543 (1993).
  - 71 P. Vajeeston, (private communication).
  - 72 F. Gygi and A. Baldereschi, Phys. Rev. Lett. **62**, 2160 (1989).
  - 73 R. Del Sole and R. Girlanda, Phys. Rev. B **48**, 11789 (1993).
  - 74 J. Thomas, G. Stephan, J. C. Lemonnier, M. Nisar, and S. Robin, Phys. Stat. Sol. (b) **56**, 163 (1973).
  - 75 C. Jouanin, J. P. Albert, and C. Gout, J. Phys. (Paris) **37**, 595 (1976).
  - 76 D. M. Roessler and W. C. Walker, Phys. Rev. **159**, 733 (1967).
  - 77 U. Schönberger and F. Aryasetiawan, Phys. Rev. B **52**, 8788 (1995).
  - 78 E. L. Shirley, Phys. Rev. B **58**, 9579 (1998).
  - 79 P. K. de Boer and R. A. de Groot, J. Phys.: Condens. Matter **10**, 10241 (1998).
  - 80 W. Y. Ching, F. Gan, and M.-Z. Huang, Phys. Rev. B **52**, 1596 (1995).
  - 81 W. H. Strehlow and E. L. Cook, J. Phys. Chem. Ref. Data **2**, 163 (1973).
  - 82 H. F. Franzen, J. Merrick, M. Umaña, A. S. Khan, D. T. Peterson, J. R. McCreary, and R. J. Thorn, J. Electron Spectrosc. Relat. Phenom. **11**, 439 (1977).
  - 83 J. H. Weaver, M. Gupta, and D. T. Peterson, Solid State Commun. **51**, 805 (1984).
  - 84 C.-Y. Xiao, J.-L. Yang, K.-M. Deng, Z.-H. Bian, and K.-L. Wang, J. Phys.: Condens. Matter **6**, 8539 (1994).

- <sup>85</sup> S. Baroni, G. Pastori Parravicini, and G. Pezzica, Phys. Rev. B **32**, 4077 (1985).
- <sup>86</sup> P. K. de Boer and R. A. de Groot, Eur. Phys. J. B **4**, 25 (1998).
- <sup>87</sup> F. C. Brown, C. Gähwiler, and H. Fujita, Phys. Rev. B **2**, 2126 (1970).